Indian Journal of Chemical Technology
Vol. 21, May 2014, pp. 168-175

Corrosion behaviour of AA2014 aluminium alloy-cenospheres syntactic foam in 3.5% NaCl solution

I B Singh*, D P Mondal, M Singh, Anshul Bhadkul & Nidhi Jha

CSIR-Advanced Materials and Processes Research Institute, Hoshangabad Road, Bhopal 462 026, India

Received 18 December 2012; accepted 20 January 2014

Corrosion behaviour of as-cast cenospheres reinforced AA2014 Al-alloy syntactic foam has been compared with that of as-cast virgin alloy (AA2014 Al-alloy) in 3.5% NaCl solution. The corrosion studies of these materials through electrochemical measurements indicate that the syntactic foam exhibits less corrosion rate when it contains up to 40 vol% of cenospheres. It is observed that the corrosion rate is further reduced with increase in cenosphere size from 75 µm to 125 µm. A detail corrosion mechanism has been presented schematically and discussed in the light of cenosphere size and volume fraction in the syntactic foam.

Keywords: Al alloy- cenosphere foam, Corrosion, Metal matrix composites, Polarization

Aluminium foam has emerged as a promising material for various applications such as energy absorption, blast resistance, vibration and sound attenuation, filters, fire retardation, heat exchangers and light weight sandwich panels[1-5]. Thus, it had found its applications in automobile, energy, defence, aerospace and general engineering sectors[6-9]. The major problems associated with these aluminium foams are (i) higher cost of manufacturing, (ii) complex shape, (iii) poor reproducibility and repeatability in foam characteristics and (iv) non-uniformity in cell size and its distribution. Furthermore, the cells are significantly coarser in size, and the size varies in a wide range[10-12]. These aluminium foams contain 80 - 95% porosity and their collapse strength (plateau stress) and modulus become considerably less[5]. Because of very low strength and modulus, bare foams are hardly used. Therefore, attempts are being made to make high strength syntactic aluminium foams where pores (micro-balloons) of different sizes and strengths, in varying volume fractions, are assembled in an aluminium alloy matrix to have desired strength and stiffness[13]. Different types of micro-balloons could be used depending upon ones requirement. These micro-ballons may be made of metallic materials or ceramics[14,15]. Thus, the micro-balloons reinforced syntactic aluminium foams are similar to that of ceramic particle reinforced composites. The major difference between these two materials is that the composites are made off dense ceramic particles, whereas the reinforcements in syntactic foams are hollow spherical in nature (micro-balloons). Because of the hollow nature of these micro-balloons, syntactic foam also exhibits excellent damping capacity as compared to the dense alloys or composites, both in terms of mechanical and acoustic damping[16-18]. The combination of high strength, higher damping capacity, better thermal stability and higher electromagnetic shielding effect, makes the aluminium syntactic foams to be a potential material for electronic packaging, as crash worthiness and vibration control, electromagnetic shielding, light-weight structural components especially for automobile, aerospace and naval applications.

Because of its great potential to be used in automobile and naval applications, there is an immense need to evaluate its corrosion behaviour in marine atmosphere. But such studies are lacking. In fact, contradictory reports on the corrosion behaviour of Aluminium matrix composites with respect to the virgin alloy are found in the literature[19-25]. Some investigators reported that the corrosion rate of composite is higher[19,20]. This is due to increase in interfaces owing due to the presence of reinforcement and greater potential difference between reinforcing particle and the matrix. Others reported that composite showed better corrosion resistance[21-23].

*Corresponding author.
E-mail: ibsingh58@yahoo.com

This is attributed to decrease in the overall exposed area of the matrix to the corrosive environment. Additionally, the reinforcing agents prevent the growth of the pits which leads to shallower and finer pits in composites as compared to that in alloy. Some investigators also reported that composite showed comparative corrosion rate to that of virgin alloy[24,25]. This is attributed to synergic effect of the above two facts. It is understood that matrix microstructure, and the type, shape and size of reinforcements play important role to govern the corrosion behaviour of aluminium matrix composites. The corrosion rate of age-hardened AA2XXX series of alloys is relatively higher and it could be improved by laser surface melting[26], making chromate passivated surface[27], friction stir melting[28], sol gel coating with CeO_2[29] and using inhibitor like $CeCl_3$, and $LaCl_3$[30]. We have also examined improved corrosion resistance of composites as compared to the alloy in as-cast condition[21] So far, to the best of our knowledge, no studies have been carried out on the corrosion behaviour of aluminium-cenosphere syntactic foam. But, very limited studies have been conducted on the corrosion behaviour of closed cell Al foams. Zhang *et.al*.[31] reported that Al-Mg-Re foam exhibits better corrosion resistance than that of Al-foam and Al-Cu alloy foam. In the present study, the corrosion behaviour of stir-cast cenosphere reinforced AA2014 Al-alloy syntactic foam (i.e AA2014-Cenosphere syntactic foam) has been compared with that of as-cast AA2014 alloy in 3.5 wt% NaCl solution at room temperature (25°C) employing open circuit potential (OCP), partial potentio-dynamic and electrochemical impedance spectroscopy (EIS) techniques. The effects of size and volume fraction of cenospheres on the corrosion behaviour of AA2014-Cenosphere syntactic foam are examined. Finally the corrosion mechanisms in these materials are understood from the micrographs of corroded surfaces and prevailing electrochemical reactions.

Experimental Procedure

Synthesis of materials

AA2014-cenosphere syntactic foam was prepared using stir-casting technique. The process involved melting of alloy, cleaning and drossing of the alloy melt, distribution of preheated cenospheres in the melt through mechanical stirring and finally casting of the alloy-cenosphere melt mixture in a preheated cast iron die having dimension of 15 mm diameter and 200 mm length. Process detail has been reported elsewhere[17]. In this study, the cenospheres size and their volume fraction have been varied. The average sizes of cenospheres selected for this study were 75 and 125 μm. The volume fraction of cenospheres varied in the ranges of 30-45%. The composition of the matrix alloy (AA2014) is as follows; Si 0.76 wt%, Fe 0.06 wt%, Cu 4.7 wt%, Mn 0.78 wt%, Mg 0.47 wt%, Cr 0.01 wt%, Zn 06 wt%, Ti 0.03 wt%, Al 93.13 wt%.

Materials characterisation

The virgin alloy and the syntactic foams were characterised in terms of microstructural characteristics, density and porosity. The microstructural characteristics include volume fraction of cenospheres, microphotographs of cenospheres and cenosphere shells and distribution of cenospheres in the matrix. For microstructural characterisation, the specimens cut from the cast fingers were polished and etched using standard metallographic technique. Keller's reagent was used for etching the polished samples. Prior to SEM examination, etched samples were sputtered with gold. For taking the micrographs of cenospheres, the required cenosphere grades were sticked to the double sided carbon tape which was then mounted on specimen holder of SEM. The average diameter of cenosphere was measured from the dimension measured on randomly selected 200 cenospheres. The chemical composition and XRD of cenospheres were examined and reported elsewhere[32,33]. The volume fraction of cenospheres and the porosity fraction of ASF were measured using standard methodology and reported relations are explained elsewhere[17].

Corrosion studies

Before carrying out electrochemical measurement, specimens of dimensions 25 mm × 10 mm × 2 mm were made. Specimens of similar dimensions were prepared from the base (AA2014) alloy. Five types of specimens designated as i) base alloy AA2014 as such, ii) AA2014- 30 vol% cenospheres, 75 μm in size iii) AA2014- vol 30% cenospheres, 125 μm in size, iv) AA2014- 40 vol% cenospheres, 125 μm in size and v) AA2014- 45 vol% cenospheres, 125 μm in size, were prepared for the corrosion studies. All the specimens were polished mechanically using standard metallographic processes and degreased with trichloroethylene prior to the experiment.

The electrochemical measurements like open circuit potential (OCP), potentiodynamic polarizations and impedance measurements were performed in

3.5 wt% NaCl solution at room temperature (25°C) using a Solartron 1280 Z corrosion measurement system. Three electrodes system, namely a working electrode (area 1 cm^2), a platinum counter electrode (area 2 cm^2) and a saturated calomel electrode (SCE) as a reference electrode were employed in the present investigation. Open circuit potential (OCP) variations with time were recorded up to 30 min of exposure. Afterwards, Tafel plot was obtained by carrying out partial potentiodynamic polarization in the potential range ± 150 mV from OCP at the potential scan rate of 1 mV/s. EIS analysis was made in the frequency range 0.1 Hz – 20 kHz using a sinusoidal a.c signal of 10 mV at the open circuit potential. The reproducibility of the electrochemical test was verified by carrying out three measurements on a fresh polished specimen. All the measurements have been performed in aerated solution under static condition. Different parameters of polarization curves and impedance diagrams were derived from software Corrware2 and Zplot respectively using curve fitting method.

After completion of EIS measurement, the corroded samples were cleaned properly and used for microstructural examination. The microstructure of the corroded specimens was examined in Scanning Electron Microscope (Jeol, JSM 5600)

Results and Discussion

Materials and microstructure

The microstructure of the cast alloy is shown in Fig. 1 (a). It is noted that the cast alloy exhibits dendritic structure of α-aluminium and interdendritic eutectic phase of α-Al and $CuAl_2$. The secondary arm spacing of this alloy is found to be around 100 µm. As the casting is made in cast iron permanent die, the solidification rate is relatively higher (~100°C/min). The microstructures of the Al- cenosphere syntactic foam with finer and coarser cenospheres are shown in Figs 1(b) and (c) respectively. It is revealed from both figures that the cenospheres are distributed quite uniformly, irrespective of the size of cenospheres. The interface between the cenospheres and the matrix is shown to be quite intact (with weak bonding in limited areas). These cenospheres mainly contain alumina-silicate phases (mullite and sillimanite) and minor amount of ferro-silicates, quartz. These phases are electrically and thermally nonconductive and inert to saline water. The variation in microstructure with the addition of cenospheres in varying amount and size may affect the corrosion behaviour of the material. The plateau stress (yield stress) of these Al-cenosphere syntactic foams has been measured (Table 1). It is noted that Al-cenosphere syntactic foam exhibits quite high strength as compared to the conventional foam and thus there is ample opportunity to use these foams in vibration and noise control and in high strength light weight structures.

Corrosion behaviour

OCP variations with time

OCP variations with exposure time recorded for all the six types of specimens are shown in Fig. 2. It can be noted that the base alloy AA2014 and AA2014-45 vol% cenospheres [samples no (i) & (v)] show their OCP quite positive as compared to remaining specimens. 45 vol% cenospheres

Table 1—Plateau stress (yield stress) of these Al-cenosphere syntactic foam

Samples No.	Materials	Plateau stress MPa
(i)	AA2014 as cast alloy	240±8
(ii)	AA2014-30 vol% cenosphere (75µm))	160±10
(iii)	AA2014-30 vol% cenosphere (125µm)	145±11
(iv)	AA2014-40 vol% cenosphere (125µm)	120±8
(v)	AA2014-45 vol% cenosphere (125µm)	110±7

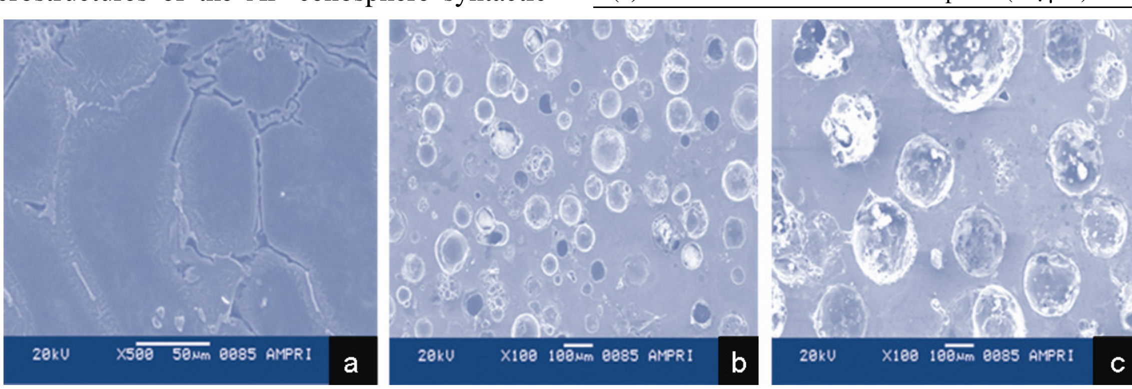

Fig. 1—Microstructure of as-cast AA2014 Al alloy (a), Al-cenosphere syntactic foam with finer cenospheres (b), and coarser cenospheres (c)

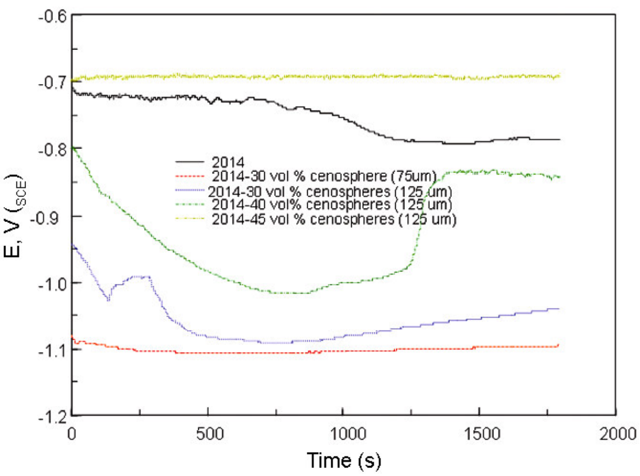

Fig. 2—OCP behaviour of base alloy and syntactic foams with time in 3.5%NaCl solution

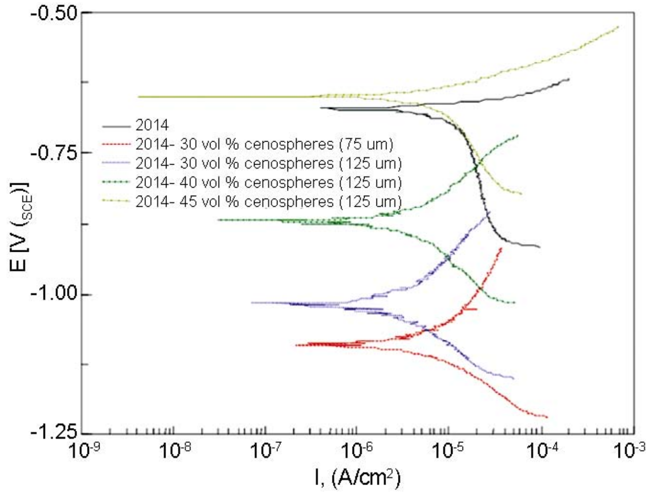

Fig. 3—Ptentiodynamic polarization curves obtained for the base alloy and syntactic foams in 3.5% NaCl solution

containing specimen show around 25 mV more positive OCP than the base alloy. In case of remaining specimens, AA2014-30 vol% cenosphere of 75 µm size containing specimen [sample no (ii)] shows maximum shift of the OCP in the negative direction (-1.1 V) followed by AA2014-30 vol.% cenospheres of 125 µm in size [sample no (iii)], AA2014-40 vol% cenospheres of smaller size [specimen no (iv)] and AA2014-40 vol% cenospheres [sample no (v)]. The shift of the OCP in the negative direction is mainly due to the accumulation of negative charges at the metal surfaces. An unequal distribution of electrical charge which gives rise to the formation of an electrical double layer and an electrical potential differences[34] that seems to be responsible for shift of the equilibrium potential in negative direction. The presence of non conducting alumina-silicate phases in the cenosphere foam presumably hinder the mobility of electrons at the interfacial regions. This finally increases the accumulation of negative charges in the electrical double layer that result in the increase of potential in the negative direction. This has been discussed latter on by designing a corrosion model.

Potentiodynamic polarization

Figure 3 depicts the partial polarization curves recorded for the base alloy and its syntactic foams for the Tafel extrapolation purposes. The extrapolation of Tafel slopes is made from the potentials at which limitation of the increase of cathodic and anodic currents starts. Different electrochemical parameters viz. corrosion potential (E_{corr}), corrosion current density (i_{corr}), cathodic (βc) and anodic (βa) Tafel constants derived from the Tafel plots, are given in Table 2. A maximum of 4-5% variations in the derived results are observed in three of the experiments carried out on fresh sample under identical conditions. From the derived results, it can be noted that i_{corr} occurs in µAcm^{-2} ranges for all the tested samples. The maximum i_{corr} (9 µAcm^{-2}) is observed in AA2014-45 vol% cenospheres containing syntactic foam [sample no (v)], which is almost 40% higher than that of i_{corr} occurred in the base alloy. However, remaining samples of syntactic foams have shown lower i_{corr} than that of the base alloy. The syntactic foam containing 30 vol% cenospheres [specimens no (ii) & (iii)] have shown around 45% less i_{corr} (~3 µAcm^{-2}) than that measured for the base alloy. Addition of 40 vol% of cenospheres [sample no (iv)] leads to an increase of i_{corr} again to 4 µAcm^{-2} . The effect of cenospheres size is another important parameter in the determination of corrosion rate. In case of 30 vol% cenospheres containing syntactic foam, one can find nearly 10% higher i_{corr} for 75 µm size cenospheres containing sample than one containing 125 µm size cenospheres. The presence of finer sizes of cenosphere particles increases the interfacial surface areas and thus results in an increase of the corrosion rate. The measured corrosion current is found well in accordance with the corrosion potential variation with time.

Measurement of comparatively a higher value of βc in the base alloy indicates the occurrence of more pronounced diffusion controlled cathodic reaction i.e. oxygen reduction reaction, as shown below:

$$H_2O + ½ O_2 + 2 e^- \rightarrow 2 OH^- \quad \ldots (1)$$

Table 2—Electrochemical parameters for different materials derived from Tafel plots

Electrochem parameters	Sample (i)	Sample (ii)	Sample (iii)	Sample (iv)	Sample (v)
E_{corr}, mV	-674	-1090	-1017	-870	-651
i_{corr}, µA/c m^2	6.65±0.3	2.90±0.16	2.85±0.15	4.20±0.21	9.32±0.5
βa, mV/decade	30±2	65±3	56±3	47±2	45±2
βc, mV/decade	87±5	55±3	58±3	62±3	66±4

Reduction in the cathodic reaction could have reduced the corrosion rate of the base alloy as compared to syntactic foams. However, occurrence of lower value of βa (Table 2), increases the resulting corrosion rate of the base alloy. In case of 75 µm size cenospheres containing syntactic foam [sample no (ii)], occurrence of a higher value of βa decreases its corrosion rate substantially as compared to corrosion rate measured for the base alloy. This is because of the anodic reaction, as the oxidation of Al to Al^{3+} becomes somewhat more pronounced in 75 µm size cenospheres containing syntactic foam [sample no (ii)]. Decrease in βa values with the increase in cenospheres volume [samples (iii), (iv), (v)] appears to increase their overall corrosion rates (Table 2). Once hydrolysis reaction starts, corrosion reaction can proceed by oxidation of Al to Al^{3+}, resulting in $Al(OH)_3$ formation as per the following reaction:

$$Al^{3+} + 3\ OH^- \rightarrow Al(OH)_3 \quad \ldots (2)$$

The resulting corrosion product [$Al(OH)_3$] makes an amorphous type white precipitates which were observed visually after the completion of polarization.

EIS measurements

Complex impedance (Nyquist diagram), Bode amplitude and phase angle plots were recorded for all the test samples at OCP after 30 min of immersion. In the Nyquist plot (Fig. 4), one can find the imaginary part of the impedance (Z'') against real part (Z') in the form of a depressed capacitive-resistive semi-circle for the base alloy and also for the cenospheres containing syntactic foams. However, depression in the semicircle is found to be more pronounced in 45 vol% cenospheres containing syntactic foam and in the base alloy. Due to the occurrence of one semi-circle in the Nyquist plot, Randles circuit consisting of resistor connected in series to a parallel connected resistor and capacitor, has been used for data analysis. EIS related parameters like charge transfer resistance (R_{ct}), double layer capacitance (C_{dl}) and solution resistance (R_s) were derived by curve fitting method (Table 3). EIS data exhibit low R_{ct} (621 Ω cm^2) for the base alloy and highest R_{ct} (1205 Ω cm^2) for the 30 vol% cenospheres (125 µm in size) containing syntactic foam. However, C_{dl} values for the syntactic foams and base alloy found to be almost in the same order. The double layer capacitance is one of the important electrochemical parameters as it measures the penetration of electrolyte through the surface layer[35-37]. Due to water intake, it reduces the resistance of the surface film. The observed R_{ct} values are well in the accordance with the i_{corr} measured from the Tafel plot. It can be inferred that the addition of cenospheres in the base alloy up to certain level decreases their corrosion rate. However, addition of cenospheres beyond 40 vol% starts increasing their corrosion rates.

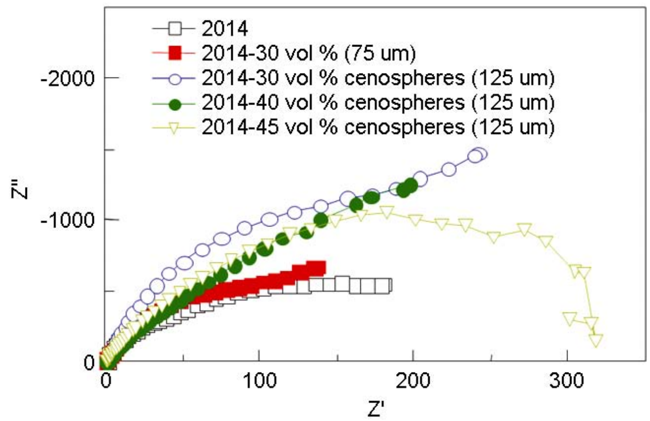

Fig. 4—EIS diagram (Nyquist plot) obtained for the base alloy and syntactic foams in 3.5% NaCl solution

Microstructural studies of corroded samples

The surface morphology of the test specimens after completion of Tafel plots was seen by SEM. SEM micrograph [Fig. 5(a)] of the base alloy after to Tafel measurement shows the grain boundaries surrounding aluminium dendrites are deeply corroded. Additionally, within the Al grains, a number of micropits are also seen in the photomicrograph. The oxide film present on the corroded surface is quite thin in its appearance. The surface of the syntactic foam containing 45 vol% cenospheres prior to Tafel

Table 3—Different parameters with % error derived from EIS measurement on different materials

EIS parameters	Sample (i)	Sample (ii)	Sample (iii)	Sample (iv)	Sample (v)
R_s, Ωcm^2	14±6%	10.2±7.5%	12.2±9%	13.2±9%	9.1±7%
C_p, uF/c m^2	12±6.8%	5.5±7.5%	5.2±6.9%	8.6±9.2%	13±8.5%
R_p, Ωcm^2	461±7.8%	675±9.1%	1205±9.8%	665±9.6%	330±9.2%

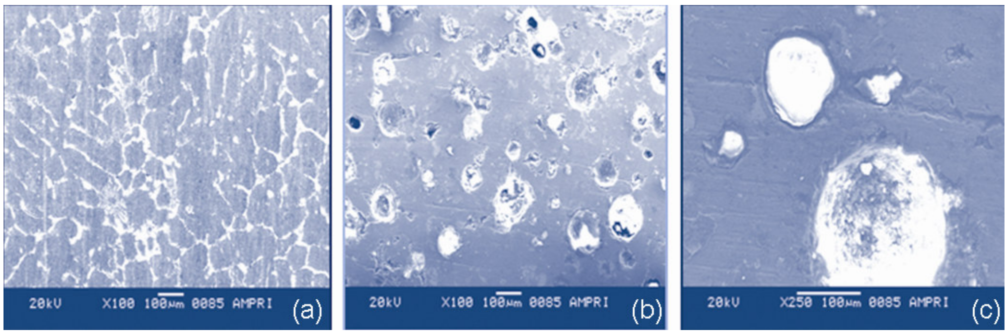

Fig. 5—SEM photomicrographs of the base alloy after polarization (a), and syntactic foam after polarization in 3.5% NaCl at different magnifications (b & c)

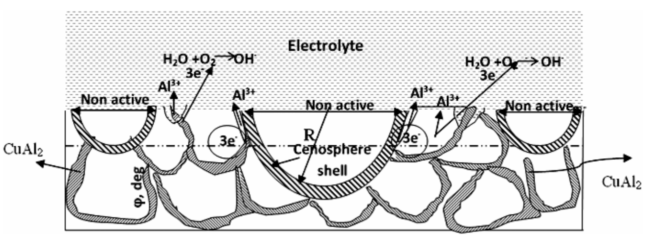

Fig. 6—Schematic description of corrosion mechanism of the syntactic foam

measurement [Fig. 5(b)] shows a large number of cenospheres imbedded in alloy matrix. Some of the cenospheres are broken at the outer surface and appeared as deep holes within the matrix . The corrosion attack can also be seen through the interfacial region of the imbedded cenospheres [Fig. 5(c)].

Corrosion mechanism model of syntactic foam

Based on the above observations, a corrosion model of cenospheres containing Al syntactic foam has been explained schematically in Fig. 6. According to this model, the active area responsible for corrosion attack gets reduced substantially due to the presence of non-conducting cenosphere particles in the matrix. However, the interfacial areas between the Al matrix and the cenosphere shell is relatively more active because of weak incoherent interfacial bonding which allow greater, depth of penetration of the electrolyte. However, the most severe region for the corrosion attack is interdendritic region containing $CuAl_2$ phase, because of a significant galvanic potential difference between this phase and matrix. The corrosion reactions in different region are also shown in the model. It is clear that Al from the matrix and interfacial region gets oxidised to Al^{3+} after releasing $3e^-$, which were consumed by the dissolved oxygen present in the electrolyte as per reaction 1. The released electrons move uninterruptedly from the matrix towards electrolyte . However, the mobility of a fraction of the released electrons at cenosphere shell-matrix interface presumably get hindered due to adjoining non-conducting cenosphere shell. This leads to accumulation of electrons at the interfacial sites that appears to be the reason for the shift of the corrosion potential in cathodic region as observed during OCP measurement (Fig. 2). In addition, this also reduces the reduction of oxygen in the electrolyte [Eq. (2)]. Therefore, the cathodic reaction slows down which finally reduces the corresponding anodic reaction i.e. oxidation of Al as described in the model. This is the reason for the fact that the presence of non-conducting cenosphere particles is ultimately responsible for the decrease in corrosion rate of the syntactic foam.

Volume fraction and size of the cenopsphere particles also play a major role in the determination of corrosion rate of the syntactic foam. This is attributed to the fact that non-active areas and interfacial areas between cenosphere and matrix vary significantly with cenosphere size and volume fraction, which could be derived and expressed by the following relations:

$$A_a = (1-V_c)A_t \quad \ldots (3)$$

$$A_{ic} = 3V_c/r_c \quad \ldots (4)$$

where A_a is the active apparent exposed area responsible for corrosion, V_c the volume fraction of cenosphere; A_t , the total area of the sample exposed to the electrolyte, A_{ic} , the interfacial area between cenosphere and matrix per unit volume of the syntactic foam; and rc, the radius of the cenosphere in the syntactic foam. These relations clearly demonstrate that the active area and the active interfacial areas between cenosphere and matrix increases with increase in cenosphere volume fraction and decrease in cenosphere size.

Since AA2014-30 vol% cenospheres of 75 µm containing foam possesses higher interfacial areas than the one containing 125µm size of cenospheres, it shows more corrosion rate and less charge transfer resistance (Tables 2 and 3). In case of 45 vol% cenospheres containing syntactic foam, both the apparent non- active area and interfacial area increase as per the Eqs (3) & (4) and their combined effect leads to relatively higher corrosion rate.

Conclusion

- Addition of cenospheres up to 40 vol% to the base alloy is found to reduce the corrosion rate of the syntactic foam in 3.5 wt% NaCl solution. Addition beyond this proportion of cenospheres in the syntactic foam increases their corrosion rate than in base alloy.
- Sizes of cenosphere particles also play a major role on the corrosion behaviour of the syntactic foams. Presence of finer size of cenospheres increases the interfacial area vis-a-vis the corrosion rate.
- Cenosphere particles in the syntactic foam shift the corrosion potential in more negative direction. This leads to decrease in corrosion reaction, responsible for the decrease in corrosion rate of the foam.
- Presence of more interfacial sites and voids near the imbedded cenosphere particles increases their corrosion reaction when cenospheres content in the foam increases beyond 40 vol%. At lower volume fraction of cenospheres the effect of non active area dominants over that of interfacial area towards the determination of overall corrosion reactions.

References

1 Andrews E, Sanders W & Gibson L J, *Mater Sci Eng A,* 270 (1999) 113.
2 Duarte I, Mascarenhas J, Ferreira A & Banhart J, *Key Engineering Materials,* 230 (2002) 96.
3 Benedyk C J, *Light Metal Age,* 4 (2002) 24.
4 Gergely V & Clyne T W, *Acta Mater,* 52 (2004) 5047.
5 Idris M I, Vodenitcharova T & Hoffman M, *Mater Sci Eng A*, 517 (2009) 37.
6 Gibson L J & Ashby M F, *Cellular Solids: Structure and Properties*, 2nd edn (Pergamon Press, Oxford), 2000.
7 Makai T, Miyoshi T, Nakano S, Somekawa H & Higashi K, *Scripta Mate,* 54 (2006) 533.
8 Banhart J & Prog J , *Mater Sci,* 46 (2001) 559.
9 Raun D, Lu G, Chen F L & Siores E, *Compos Struct,* 57 (2002) 331.
10 Kritzt B, Martin U & Mosler U, in *Handbook of Cellular Metals: Production, Processing, Applications,* edited by Degicher Hans Peter & Kriszt Brigitte (Verlay GmbH 69469, weinheim) 2002.
11 Simone A E & Gibson L J, *Acta Mater*, 46 (1999) 3109.
12 Gibson L J & Ashby M F, *Cellular Solids: Structure and Properties* (Cambridge University Press, Cambridge, New York), 1997.
13 Kiser M, He M Y & Zok F W, *Acta Mater*, 47 (1999) 2685.
14 Balch D K & Dunand D C, *Acta Mater*, 54 (2006) 1501.
15 Sugimura Y, Meyer J, My H, Smith H P, Grensted J & Evans A G, *Acta Mater* , 45 (1997) 5245.
16 Balch D K, O'Dwyer J G, Davis G R, Caby C M, Gray G T & Dunand D C, *Mater Sci Eng* A, 391 (2005)408.
17 Wu G H, Dou Z Y, Jiang L T & Cao J H, *Mater Lett,* 60 (2006) 2945.
18 Wu G H, Dou Z Y, Sun D L, Jiang L T, Ding B S & He B F, *Scripta Mater,* 56 (2007) 221.
19 Modi O P, Saxena M, Prasad B K, Yagneswaran A H & Vaidya M L, *J Mater Sci*, 27 (1992) 3897.
20 Yao H Y & Zhu R Z, *Corros Sci*, 54 (1998) 499.
21 Singh I B, Mondal D P, Singh M & Das S, *Corros Sci* , 51 (2009) 234.
22 Pinto L &Zshech E, *Mater Sci Forum,* 217-222 (1996) 1593.
23 Sun H, Koo E Y & Wheat H G, *Corrosion,* 47 (1991) 741.
24 Yu S Y, Ishic H & Chung T H, *Met Mater Trans A,* 27 (1996) 2653.
25 Tsutsuii M &Yamada Y, *J Jpn Inst Met,* 56 (1996) 271.
26 Watkins KG, Liu Z, McMahon M, Vilar R & Ferreir M G S, *Materials Sci Eng A,* 252 (1998) 292.
27 Treacy G M & Wilcox G D, *Appl Surface Sci*, 157 (2000) 7.
28 Surekha K, Murty B S & Rao K P, *Materials Design,* 32 (2011) 4502.
29 Schem M, Schmidt T, Gerwann J, Wittmar M, Veith M, Thompson G E, Molchan I S, Hashimoto T, Skeldon P, Phani A R, Santucci S & Zheludkevich M, *Corros Sci,* 51 (2009) 2304.
30 Mishra A K & Balasubramaniam R, *Corros Sci,* 49 (2007) 1027.
31 Zhang Yong-Ming, Chu Xu-Ming, Wang Hui, He Si-Yuan & He De-Ping, *Corros Sci*, 51 (2009) 1440.

32 Jha N, Badkul A, Mondal D P, Das S & Singh M., *Tribology Int,* 44 (2011) 220.

33 Rohatgi P K, Kim J K, Gupta N, Alaraj S & Daoud A, *Composite Part A,* 37 (2006) 430.

34 Shreir L L, Corrosion *Vol 1 : Metal /Environment Reactions*, 2^{nd} edn (Newnes-Butterworth, London), 1976

35 Meticos H , Tkaice E, Kwokal A & Piljac J, *Surf Coat Technol,* 165 (2003) 40.

36 Keddam M, Kurtz C, Takenouti H, Schuster D & Zuili D, *Electrochim Acta*, 42 (1997) 87.

37 Ruhi G, Modi O P, Singh I B, Jha A K & Yegneswaran A H, *Surf Coat Technol,* 201 (2006) 1866.